Data science meets Astrophysics in the Orion B Molecular Cloud

NGUYEN Thi Kim Ha[1]
Supervised by: Francois LEVRIER[2]

1: MAUCA – Master in Astrophysics, Observatoire de la Côte d'Azur/Université Côte d'Azur, Bât. Fizeau, Parc Valrose, 06100 Nice, France – email: ha.nguyen@oca.eu
2: LPENS, ENS, Université PSL, CNRS, Sorbonne Université, Université de Paris, Paris, France

Abstract

The interstellar medium (ISM) is a complex non-linear system because of an effect of interplay between gravity and magnetohydrodynamics. To understand how it works, we progress through the quantitative comparison between observations and simulations. To do this, we need a comprehensive and generic (*i.e.* flexible) statistical description of the structures. Hence, the comparison is based on this statistical description between observations and simulations are reliable to understand the ISM physics. We start from the Wavelet Scattering Transform (WST), a low-variance statistical description developed from real-valued time series and image data for use in machine learning and deep learning applications [4]. Then, we reduce the WST via a fit of its angular dependencies, containing virtually the same information as the WST information in the form of a few terms, whose physical interpretations are straightforward. They encode in particular statistical isotropy or anisotropy. The Reduced Wavelet Scattering Transform (RWST) is also a statistical description with a smaller number of coefficients than the WST describing complex structures arising from non-linear phenomena. We apply this description to the Orion-B molecular cloud with the observed data of ^{12}CO, ^{13}CO and C^{18}O. In this report, we concentrate to apply it to column density maps of different regions within the entire field. The first result we obtain is the evidence for spatial variations, as not all subsets give the same results. The second one is a study of the noise that rapidly contaminates RWST coefficients and the results are thus robust since it would take only a small amount of noise to destroy the signal.

Keywords: Column density, WST, RWST, isotropic, anisotropic

1 Introduction

Stars form exclusively within molecular clouds. This is a result of low temperatures and high densities, since the gravitational force acting to collapse the cloud must exceed the internal pressures that are acting "outward" to prevent a collapse. The structure of a giant molecular cloud (GMC) is a complex pattern of filaments, sheets, bubbles, and irregular clumps. The densest parts of the filaments and clumps are traced with CO rotational lines. Understanding star formation requires understanding how the interstellar medium (ISM) works.

The ISM is the material that fills the space between the stars. This is made up of physical and chemical phases such as dense ($n_H = 10^3 \rightarrow 10^6$ cm^{-3}) versus diffuse gas ($n_H = 100$ cm^{-3}), hot ($n_H = 0.6$ cm^{-3}, $T \sim 5000K$) versus cold gas ($n_H = 30$ cm^{-3}, $T \sim 50K$), ionised, atomic, or molecular gas and gravitationally bound versus free-floating gas [3]. It is the non-linear physics that leads to the complex, non-Gaussian, ISM structures such as filaments. Its physics involves a highly non-linear interplay of gravity, magnetohydrodynamics and thermodynamical processes coupled to microphysical processes [6]. We understand more via observations, numerical simulations, and phenomenological models but do not have a comprehensive model of the ISM. We may resort to phenomenological models. Our approach is to study structures statistically, independently of a model. It is the tool for comparing observations with complex numerical simulations. If the two give the same statistics, we are confident the simulation is right. However, the process of simulations are so complicated, we select some physics instead of others like gravity, thermal instability, turbulence,...Because of the complex non-linear physics in the ISM, we need to characterize accordingly non-Gaussian processes.

The Orion B molecular cloud is an approximation 20 parsec star-forming complex in the constellation Orion at a distance of about 1300 light-years. It is one of the closest regions of massive star formation. Through the glow of dust at far-infrared wavelengths and radiation from newborn stars, a network of interstellar filaments is revealed. Molecules radiate in the different lines, mostly rotational lines at millimeter wavelengths. The abundances and excitation vary, thus the line emission also varies. We

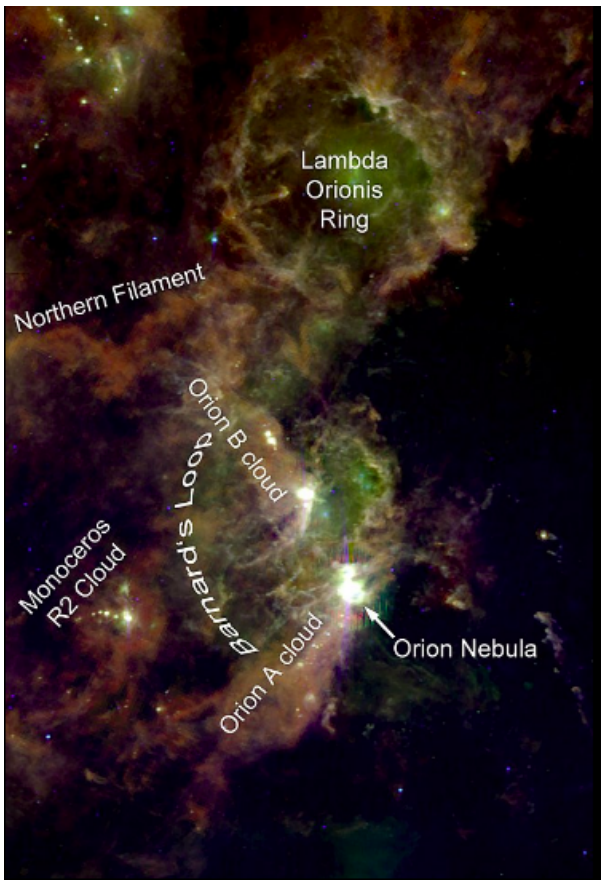

Fig. 1. The Orion Molecular Cloud Complex [12].

want to use these lines to determine the physical and chemical conditions in the emitting gas. The wide-field mapping of Orion B gives accurate three-dimensional maps (position-position-velocity or frequency) of the molecular structure.

Column density maps of molecular clouds are one of the most important observables in the context of molecular cloud and star formation studies. Dust thermal emission is the best tracer of the bulk of material in molecular clouds, assuming a fixed ratio between the gas content, *i.e.* its column density and the dust emission.

The basis of the description of these maps is the wavelet transform. The important feature of this transform is to separate the variability of processes at different scales in a hierarchical manner [5]. This means that the interactions of small-scale structures create local structures at intermediate scales, which then interact to lead to structures at larger scales [1]. The Wavelet Scattering Transform (WST) [4] is able to formalize this hierarchical approach for non-Gaussian fields using a 2D multiresolution framework granted by the wavelet transform. It is able to do so while keeping a reduced variance, which means that the difference when applying the WST to different fields generated by the same process is small, *i.e.* the WST does not depend strongly on the details of the field, but only globally on its statistics. The outputs of the WST are called *scattering coefficients*. They are a statistical representation of the field with low-variance and low-dimension.

The RWST is indeed a reduction in dimensionality from the WST, stemming from the empirical finding that angular dependencies of WST coefficients are regular and can be modeled simply using cosine functions. This means that all of the information in the WST components is contained in the form of a few terms whose physical meanings are relatively simple to interpret. For example, the number of WST coefficients may be of the order of 1000 and for RWST coefficients, there are fewer than 100.

2 Data

The Orion molecular clouds surrounding the Horsehead nebula were observed at the IRAM-30m telescope by the ORION-B project [9] from August 2013 to November 2019. The frequency coverage from 84 to 116 GHz was sampled at 200 kHz spectral resolution. The large bandwidth covers 20 chemical species at a sensitivity of 0.1 K per channel. The field of view is 0.81 × 1.1 deg towards the Orion B molecular cloud part that contains the Horsehead nebula, and the HII regions NGC 2023, NGC 2024, IC 434, and IC 435 in Fig.2. The angular resolution ranges from 22.5" to 30.5". The H_2 is the most abundant molecule in the ISM, but having no permanent dipole moment, it is difficult to observe

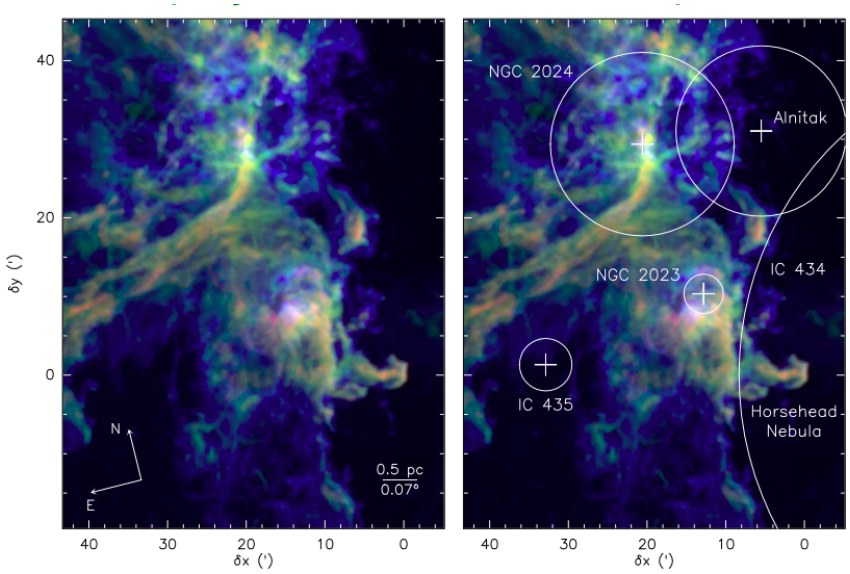

Fig. 2. The south-western edge of the Orion B molecular cloud include: Alnitak, σOri, IC 434, IC 435, NGC 2023, NGC 2024 and Horsehead [9].

directly in dense and cold clouds, so surveys generally use the second most abundant molecules, *CO*, whose rotational transitions are observable. The *CO* shows us the molecular anatomy of the Orion B, complemented by the gas column density N_H that is obtained from the dust [8] and the FUV radiation field derived from WISE data at 12 μm [3]. The molecular data shown in Fig.2 describes the (1-0) line of the CO isotopologues ^{12}CO, ^{13}CO and C^{18}O. A position-position-frequency cube represents $1074 \times 758 \times 160000$ pixels. It is also wideband in frequency. The different isotopologues have lines at different frequencies, ^{12}CO at 115 GHz, ^{13}CO at 110 GHz and C^{18}O at 109 GHz [9].

The data of column density is derived from the Planck dust-emission maps, Herschel dust-emission maps and 2MASS NIR dust-extinction maps [8]. This data depends on the thermal emission of dust whose energy distribution depends on dust temperature, spectral index and opacity, and is correlated with hydrogen column density N_H. It is possible to derive N_H from dust emission. The line intensities are correlated with the column density [7]. The more matter along the line of sight, the brighter the lines [3].

3 Wavelet Scattering Transform

3.1 Introduction

The wavelet scattering transform is used to give a statistical description that is stable to deformation and rotation invariant if the field is statistically rotation invariant [2].

The wavelet transform allows separating scales to study long-range interactions through a hierarchical multiscale approach and the progressive identification of structure at different scales. This section explains the construction and the properties of the WST components, called scattering coefficients. The computations of the scattering coefficients can be reproduced by a software called scatnet [1].

The original goal of the WST was to reproduce the classification results obtained on images and time series by deep-learning methods. In this work, we use the WST as a global statistical diagnostics of a field whose properties are assumed to be statistically homogeneous. The WST is built by successive convolutions of the field under study with Morlet wavelets, followed by the application of the modulus operator [1].

3.2 Computation of the WST coefficients

We only apply the statistical description for a two-dimensional field $I(\mathbf{x})$. Normally, $I(\mathbf{x})$ is defined on a grid of $d \times d$ pixels, so $\mathbf{x}$ stands for a position of one point. The wavelet transform may be continuous, however here we use discrete sets. The number J is the maximum scale index for these discretized wavelets, which is related to the largest scale probed in the field $I(\mathbf{x})$. The scattering coefficients are performed in Fourier space, involving convolutions with the complex Morlet wavelets which are presented in App.A. The integer scales j are labeled from 0 to $J-1$ and related to effect sizes of 2^j pixels [1]. We assume that 2^J is smaller than or equal to the size d of the image. The angle ϑ labels the dependencies of the wavelets on an angle and is associated with

[1] https://www.di.ens.fr/data/software/scatnet/.

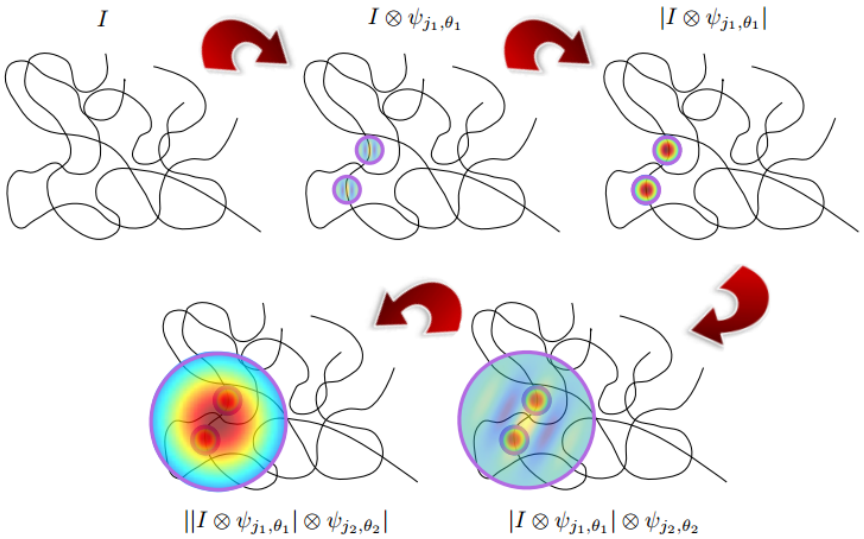

Fig. 3. Picking up correlations across scales. Layer 1 picks up structures at (j_1, θ_1). Layer 2 picks up these structures appearing together at (j_2, θ_2).

an integer θ [1]:

$$\vartheta = (\theta - 1) \times \pi/\Theta, \tag{1}$$

where Θ is the number of angles probed in a π interval. For real fields, angles ϑ are considered in [0,π) since θ runs from 1 to Θ.

The Fourier transform of a real-valued field $I(\mathbf{x})$ is such that $\tilde{I}(-\mathbf{k}) = \tilde{I}^*(\mathbf{k})$ where $*$ stands for complex conjugation. The wavevector $\mathbf{k}$ is the conjugate of an oriented scale and this oriented scale is labeled by (j, θ). The Fourier components for **-k** do not give any more information than those for **k**, we thus probe only half the Fourier plane. So, the angle θ runs from 1 to Θ. This is convenient to distinguish the scale and angular dependencies of the scattering coefficients.

An initial mother wavelet $\psi(\mathbf{x})$ is defined by the product of oscillation of unit frequency with a Gaussian window. The complex Morlet wavelets $\psi_{j,\theta}$ are defined as rotated and scaled versions of the mother wavelet [1]:

$$\psi_{j,\theta}(\mathbf{x}) = 2^{-2j} \cdot \psi(2^{-j} r_\theta^{-1} \mathbf{x}) \tag{2}$$

where r_θ is a rotation operator of angle θ.

The WST coefficients are divided into three layers, labeled by an index m going from 0 to 2. We estimate the WST coefficients for a given field $I(\mathbf{x})$ by using successive convolutions with wavelets, modulus operators and spatial integration.

The schematic is given in Fig.3 shows the steps of convolution and modulus. The circle is the support of a localized wavelet in direct space. The convolution of the field $I(\mathbf{x})$ and the first wavelet ψ_{j_1,θ_1} a non-zero signal in the regions highlighted where the structure is aligned with the wavelet. Picking up structures depends on the rotation θ_1 of wavelet and the value of j_1. The second step is taking the modulus to be sure that spatial integration is not zero. It is like a Gaussian multiplied by a redressed oscillation. Next, we perform the second convolution at a larger scale j_2 and orientation θ_2, which picks up the presence of the two small-scale blobs. Hence, the small-scale structures appear together at this location separated by this larger scale j_2 and oriented along θ_2. To perform the average value of the field, we integrate the whole field $I(\mathbf{x})$ and divide by a normalization factor,

- The first layer m = 0 gives the average value of the field and contains only one coefficient S_0 [1]:

$$S_0 = \frac{1}{\mu_0} \int I(\mathbf{x}) d^2x, \tag{3}$$

where the normalization factor μ_0 is the surface over which the integration is performed.

- The second layer m = 1 characterizes the amplitudes of spectral components of the field across the different oriented scales. They are noted S_1 for the (j_1, θ_1) oriented scale [1]:

$$S_1(j_1, \theta_1) = \frac{1}{\mu_1} \int |I \otimes \psi_{j_1,\theta_1}|(\mathbf{x}) d^2x, \tag{4}$$

where μ_1 is the normalization factor:

$$\mu_1 = \int |\delta \otimes \psi_{j_1,\theta_1}|(\mathbf{x}) d^2x, \tag{5}$$

involving the Dirac delta function δ (μ_1 is therefore independent of j_1 and θ_1).

- The third layer m = 2 is related to the modulations of small scales by other larger scales. These coefficients depend on two oriented scales, and are written $S_2(j_1, \theta_1, j_2, \theta_2)$ [1]:

$$S_2(j_1, \theta_1, j_2, \theta_2) = \frac{1}{\mu_2} \int ||I \otimes \psi_{j_1,\theta_1}| \otimes \psi_{j_2,\theta_2}|(\mathbf{x}) d^2x, \tag{6}$$

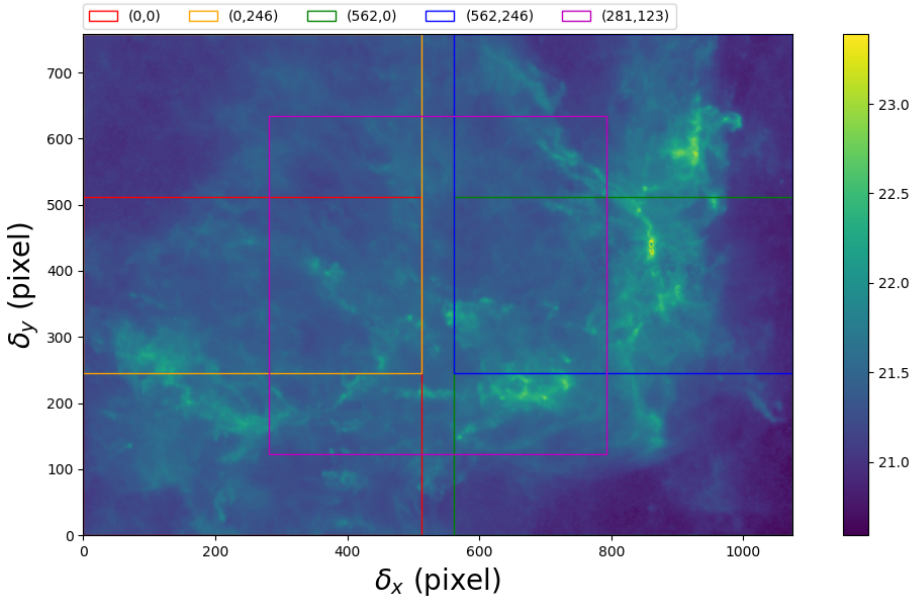

Fig. 4. The column density map of the Orion B molecular cloud [8]. The map is divided into five subsets with size 512×512 (pixels). The scale is the logarithm of N_H (cm^{-2}).

where μ_2 is defined similarly to μ_1. In Eq.6, the first oriented scale (j_1, θ_1) is modulated at a second oriented scale (j_2, θ_2) [1]. The WST coefficients depend on moments of $I(\mathbf{x})$[2]. The coefficients of layer m include information pertaining to moments of order up to 2^m [4]. These m = 2 coefficients can discriminate fields whose power spectra are identical, because the power spectrum is related to order two moments that is the Fourier transform of the auto-correlation function.

The S_2 coefficients are negligible for $j_2 < j_1$. After $|I(\mathbf{x}) \otimes \psi_{j_1,\theta_1}|$, most of the information at scales smaller than or equal to 2^{j_1} is lost. The whole information on how two scales j_1 and j_2 interact is contained in $S_2(j_1, \theta_1, j_2, \theta_2)$ for $j_2 > j_1$ and for all θ_1 and θ_2.

Moreover, we could construct scattering coefficients for deeper $m \geqslant 3$. They describe couplings between three scales or more and correlations of order higher than four. In this work, we limit our analysis to the $m \leqslant 2$ layers because the energy contained in $m \geqslant 3$ is at most a few percent of the total energy in the signal [4], as explained in App.B.

3.3 Properties and normalization of the WST coefficients

With the given J and Θ, we count the number of scattering coefficients. For layer m = 1, there are $N_1 = J \times \Theta$. For layer m = 2, the number of coefficients is $N_2 = J(J-1)/2 \times \Theta^2$. In this work, the size of the subsets we use are 512×512, so to have sufficient statistics even at large scales we take $J = 5$ and $\Theta = 8$, leading to $N_1 = 40$ and $N_2 = 640$.

[2] These moments are means of products like $\langle I(x_1) * I(x_2) * ... * I(x_n) \rangle$.

For layer m = 0, there is only one coefficient so N_0 = 1. In total, there are 681 coefficients.

Should the scattering coefficients S follow power-laws with the scale 2^j, which is an expected property of simple random fields, then plotting their logarithms as a function of j would yield straight lines. The deviations from the straight line is more conspicuous. We normalize each layer by its previous layer, and denote $\bar{S}$ these normalized coefficients [1]:

$$\log_2[\bar{S_1}(j_1, \theta_1)] = \log_2[S_1(j_1, \theta_1)] - \log_2[S_0], \quad (7)$$

and

$$\log_2[\bar{S_2}(j_1, \theta_1, j_2, \theta_2)] = \log_2[S_2(j_1, \theta_1, j_2, \theta_2)] - \log_2[S_1(j_1, \theta_1)], \quad (8)$$

with $\log_2(\bar{S_0}) = \log_2(S_0)$.

This normalization helps to separate the different layers. If the whole field is multiplied by a constant, the terms S_0, S_1, S_2 are changed by the same factor. Therefore, that will add the same additive constant to $\log(S_0)$, $\log(S_1)$ and $\log(S_2)$. By doing this normalization, we remove such an arbitrary constant. Note, this normalization is done locally before performing the spatial average [1]. If the description of the field is not statistically homogeneous, the WST can be used to achieve a local description. These local coefficients are estimated similarly to the global coefficients in Eqs.3, 4 and 6. The one difference is that spatial integration is limited to a subset of the space by a convolution with a normalized Gaussian window with fixed-width 2^J [4].

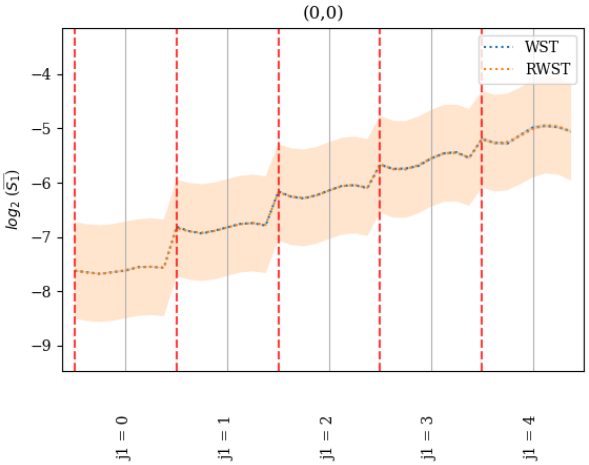

Fig. 5. Logarithms of the normalized scattering coefficients a subset of the column density map in layer m = 1. The WST coefficients and the RWST model based on the RWST coefficients are presented by blue and orange curves, respectively. The colored band shows the standard deviation of WST coefficients across the map. The red dashed lines separate the different scales j_1.

4 Reduced Wavelet Scattering Transform

4.1 Introduction

In this section, we start from the WST and build a simple statistical description called Reduced Wavelet Scattering Transform (RWST) written in terms of *reduced scattering coefficients*. These coefficients are functions of j_1 and j_2 that is determined by fitting a simple model of the angular dependency on (θ_1, θ_2) of the WST coefficients. One major point of this procedure is that it decreases the number of coefficients while keeping most of the information. For instance, there are 681 coefficients of the WST ($J = 5, \Theta = 8$), for RWST they decrease by an order of magnitude.

The WST coefficients depend on scales and orientations. If a field is statistically invariant under rotations or parity, so should the WST as a statistical description. We, therefore, expect regularities in angular dependencies. Regularities can be modeled through the Fourier series.

We consider a model of the logarithms of the normalized WST coefficients [1] which separates the dependencies on the angles and on the scales:

$$\log_2\left[\bar{S}_m(j_i,\theta_i)\right] = \sum_p \widehat{S}^p_m(j_i) \times f^p_m(\theta_i), \quad (9)$$

for m = 1,2. For m = 0, $\log_2(\bar{S}_0) = \widehat{S}_0$. The functions f^p_m is a family of functions to describe the angular dependency of the scattering coefficients on θ_i. Due to the scattering coefficients being periodic when viewed as functions of theta for a given scale, using a Fourier development is a reasonable choice. We, therefore, use cosine functions for $f^p_m(\theta_i)$, with p being the harmonic number and these functions being centered on the reference angles related to preferred directions in anisotropic fields. We limit ourselves to the zeroth and first terms (constant and cosine, respectively). The reduced scattering coefficients are the $\widehat{S}^p_m(j_i)$ that show the amplitudes of each angular dependency, and the reference angles.

4.2 Reduction of the angular dependency

Let us introduce the different angular dependencies of the scattering coefficients. We assume that the given field is anisotropic and has one preferential direction at most, *i.e.*, images of fluid flows may have a mean direction.

Starting with the layer m = 1, the angular dependency on θ_1 is modeled as [1]:

$$\log_2[\bar{S}_1(j_1,\theta_1)] = \widehat{S}^{iso}_1(j_1) + \widehat{S}^{aniso}_1(j_1) \times \cos\left(\frac{2\pi}{\Theta}[\theta_1 - \theta^{ref,1}(j_1)]\right), \quad (10)$$

where $\theta^{ref,1}(j_1)$ is a reference angle giving the direction of anisotropy. The first layer scattering coefficients are modeled as the sum of an isotropic term (dependent on the scale) without angular dependency and an anisotropic term with an amplitude also dependent on scale.

In terms of actual angles, not indices, the second term in Eq.10 reads $\cos[2(\vartheta_1 - \vartheta^{ref,1}]$, it is π periodic. The angle $\vartheta^{ref,1}$ may also be defined modulo $\pi/2$ by reversing the sign of the $\widehat{S}^{aniso}_1$ terms. This degeneracy is lifted if we impose $\widehat{S}^{aniso}_1 > 0$. If the field is statistically isotropic, the second term is expected to vanish $\widehat{S}^{aniso}_1 \simeq 0$.

For the layer $m = 2$, there are four terms includ-

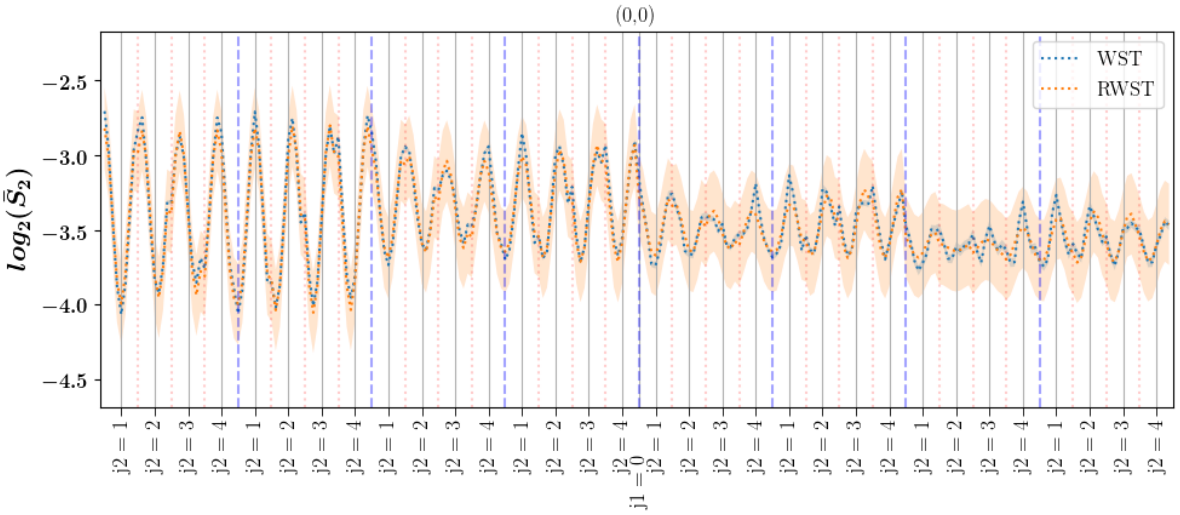

Fig. 6. Logarithms of the normalized scattering coefficients of a subset of the column density map in layer $m = 2$. The WST coefficients and RWST models are presented by blue and orange curves, respectively. Only the ($j_1 = 0$, θ_1, j_2 and θ_2) coefficients are plotted. The blue and pink dashed lines separate different angles θ_1 and scale j_2, respectively. The j_2 ranges from 1 to 4 for each θ_1. The colored band shows the standard deviation of the WST coefficients across the map.

ing two isotropic and two anisotropic [1]:

$$\begin{aligned}\log_2[\bar{S}_2(j_1,\theta_1,j_2,\theta_2)] &= \widehat{S}_2^{iso,1}(j_1,j_2) \\ &+ \widehat{S}_2^{iso,2}(j_1,j_2)\times\cos\left(\frac{2\pi}{\Theta}[\theta_1-\theta_2]\right) \\ &+ \widehat{S}_2^{aniso,1}(j_1,j_2)\times\cos\left(\frac{2\pi}{\Theta}[\theta_1-\theta^{ref,2}(j_1,j_2)]\right) \\ &+ \widehat{S}_2^{aniso,2}(j_1,j_2)\times\cos\left(\frac{2\pi}{\Theta}[\theta_2-\theta^{ref,2}(j_1,j_2)]\right),\end{aligned} \tag{11}$$

These cosine functions have the same period as in the $m = 1$ layer. The $\widehat{S}_1^{iso}$ and $\widehat{S}_2^{iso,1}$ are components indenpendent of the angles(s). For the anisotropic terms, we select the same $\theta^{ref,2}(j_1, j_2)$ as in the first layer $\theta^{ref,1} = \theta^{ref,2}$ since they may be expected to be linked to the only preferential physical direction. Also, we impose $\widehat{S}_2^{aniso,i} > 0$ to ensure this angle is in $[0, \pi]$.

The second term in Eq.11 is labeled isotropic for the following reason. Considering a field that is statistically rotation invariant and its $m = 2$ WST statistics for angles θ_1 and θ_2. Now, we consider the WST statistics of the same field for $\theta_1 + \delta\theta$ and $\theta_2 + \delta\theta_2$. The two wavelets involved in this second situation have the same relative position angle, and so the rotation invariance implies that there is a part of the WST statistics that remains unchanged in this transformation. That is what this term represents and why it is called *isotropic*.

The set of scattering coefficients is fitted by these particular angular dependencies, leading to eight functions of the scales j_1 and j_2. These form the so-called Reduced Wavelet Scattering Transform [1]. Compared to the number of WST coefficients in the previous layer, there are $3J$ RWST coefficients for layer $m = 1$ (with three functions of S_1^{iso}, S_1^{aniso} and $\theta^{ref,1}$ for which there are J values each) and $5J(J-1)/2$ RWST coefficients for layer $m = 2$ (with five functions $S_2^{iso,1}$, $S_2^{iso,2}$, $S_2^{aniso,1}$, $S_2^{aniso,2}$ and $\theta^{ref,2}$), the total number of coefficient is reduce to 66.

5 Application of the WST and RWST to the total gas column density map

5.1 Different statistics in subsets

The data we apply the WST/WRST analysis to is a 1074×758 pixels corresponding to angular size 161,1×113,7 (arcminute). Also, it is total gas density map as there are maps for the column densities of every species. From the given data in [8], the field under study is $\log(N_H)$.

We expect these statistics to depend on the position on the sky because some regions are diffuse, others are more dense, resulting in heterogeneous statistics across the area. The whole map is divided into equally sized squares with 512×512 pixels corresponding to angular size 76.8 (arcminute). There are five subsets in the Fig.4 that are not independent since they overlap. It should give us an idea of the variation of the statistics at large scales.

We consider different subsets that we can see by eye are different (some have filaments, cores, while some are more diffuse) and we want to see how this

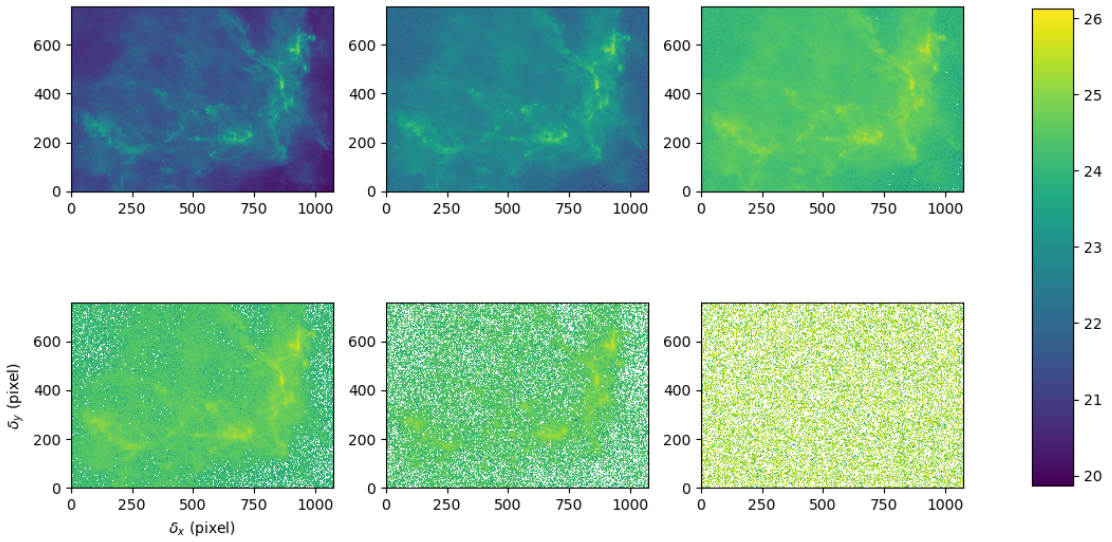

Fig. 7. The column density map in logarithmic scale with Gaussian-distributed noise added [8]. The SNR is in turn 1000, 10, 3, 1, 0.1 and 0.001 from left to right and top to bottom.

translates into the WST and RWST diagnostics.

The logarithms of scattering coefficients are shown in the Fig.5 for $m = 1$ and Fig.6 for $m = 2$. All of the components are plotted as a function of their arguments in lexicographical order (j_1, θ_1, j_2, θ_2). Because of $j_1 < j_2$, when $j_1 = 0$, j_2 starts at 1. Similarly, for $j_1 = 1$, j_2 has the values 2, 3 and 4. The scattering coefficients are shown in Fig.5 and Fig.6 display a regular pattern across the angles and scales. For the $m = 1$ coefficients, the shape is stair-like and for $m = 2$, it seems to be an oscillatory structure. This regularity results from physical constraints and allows the RWST model to compress significantly the statistical information contained in the WST coefficients. We fit the angular dependencies of the WST scattering coefficients following the cosine functional forms given in Eq.10 and 11.

The WST curves in Fig.5 and Fig.6 represent an average over the various samples obtained for a given set of angles and scales, in a given subset. Indeed, for subsets of size $512 = 2^9$, we consider scales up to $2^{J-1} = 2^4 = 16$. This WST computation being performed locally, we, therefore, have approximately $(512/16)^2 = 1024$ independent realizations (many more for smaller scales). The WST curves shown in Fig.5 and Fig.6 give the average over these various samples, and the colored bands give the corresponding statistical standard deviation. From the covariance of the optimal values, we take this square root of its diagonal to estimate a standard deviation.

Based on the Fig.5 for $m = 1$ and Fig.6 for $m = 2$, the empirical WST coefficients and the RWST model match within the error bars. This proves that the RWST captures the same information as the WST. The efficiency of this angular reduction from the WST to the RWST provides strong evidence that there is no significant loss of statistical information, along with a significant dimensionality reduction.

Statistical uncertainty comes from different WST coefficients found across the field. These are used to compute a reduced χ^2_r using the difference between model RWST and mean WST, weighted by uncertainties. The χ^2_r values are calculated independently for each subset and each scale j_1 for $m = 1$ or pair of scales (j_1, j_2) for $m = 2$.

For the $m = 1$ coefficients, in the Fig.8, we consider the χ^2_r, we see that these values are reasonable (around 1) up to $j_1 = 3$, but increase significantly (to 4 or 6 for some subsets) at the largest scales $j_1 = 4$. This means that the RWST model and empirical mean WST are not matched completely. The field is actually not statistically homogeneous at these scales, so the empirical mean is not an accurate estimate.

5.2 Effect of the noise

Typically, the measurement of received signals is contaminated by noise. Obviously, in the data we have, there is still noise. The higher the noise, the more signal is lost. The purpose of this section is to assess the effect of the signal-to-noise ratio (SNR) on the WST signal.

To the original map, we add some random noise drawn from a Gaussian distribution with a dispersion that is such that the SNR takes prescribed values. These values are 0.001, 0.1, 0.3, 1, 3, 10 and

1000 in Fig.7.

The Fig.10 shows the layer $m = 1$ RWST coefficients for one of the subsets of the map, and various levels of noise. In the absence of noise, this term increases with scale, but it is different for the different subsets, the statistics are thus not homogeneous. With some noise, $\widehat{S}_1^{iso}$ turns upwards at small scales. In the case of large noise, the power-law decrease of $\widehat{S}_1^{iso}$ with scale drowns any signal-related part for all subsets, which leads to homogeneous statistics.

The noise is drawn randomly and independently from pixel to pixel, so the effect of the noise on the WST and RWST first appears at small scale. The noise is isotropic, this is why $\widehat{S}_1^{iso}$ goes to zero as the noise increases.

Looking at Fig.10, we see that for the subset (562, 246), the anisotropic term remains positive even with very high noise. In Fig.4, this region has filaments and other brighter oriented structures. We interpret the result of Fig.10 as being due to the fact that the noise has less impact on this subset, so the anisotropic term remains somewhat significantly positive at large scales even at very low SNR. For other subsets, when the anisotropy level is not significantly different from zero,the $\theta^{ref,1}$ makes no sense.

Overall, we see that the higher the SNR, the closer curves are to the noise-free case. For scale-invariant fields, we expect $\widehat{S}_2^{iso,1}$ to depend on j_2 -j_1 instead of j_1 and j_2 separately. In particular, the noise is scale-invariant.

The scale invariance signature of the $m = 1$ and the $m = 2$ is that reduced scattering coefficients depend on j_2 - j_1 only. Indeed, in such a case, the modulation of a first scale by a second scale only depends on the ratio between both scales, but not on their absolute values. This property can be seen for instance on the components $\widehat{S}_2^{iso,i}$ and $\widehat{S}_2^{aniso,i}$ on Fig.11 in the very low SNR case, when scale-invariant noise dominates: their curves for different values of j_1 are superimposed when plotted as a function of j_1 - j_2.

The two terms $\widehat{S}_2^{aniso,1}$ and $\widehat{S}_2^{aniso,2}$ and the associated $\theta^{ref,2}$ reference angle characterize the anisotropies of the field under study. These terms are comparable to the $m = 1$ anisotropic component. They are shown in Figs.16 and 17 whose values are smaller than $\widehat{S}_2^{iso,i}$, with the maximum value is 0.1. We know that they vanish for fields that are isotropic.

6 Conclusion

In this work, we applied a low-dimensionality statistical description of complex structures arising from non-linear phenomena to observational data related to the Orion B Giant Molecular Cloud. The WST is a low-variance statistical description of non-Gaussian processes via a hierarchical multiscale approach based on the wavelet transform. We reduced the WST by fitting angular dependencies and keeping most of the information into a small number of coefficients. These coefficients describe isotropic and anisotropic terms, the latter vanishing if the field is isotropic.

The RWST is of interest to characterize non-Gaussian physical processes. We choose $J = 5$ and $\Theta = 8$ based on the data we produced, there are 66 RWST coefficients from 1074×758 map instead of 681 WST coefficients. The accuracy of the description of non-linearities rests on the fact that these statistical descriptors encode moments of order up to four, have reduced variances, and properly characterize the couplings between scales [1].

This statistical description is advantageous for homogeneous, noise-free processes. Nevertheless, some caveats should be noted when applying the method to observational data. In the sky-observing area, obviously without uniformity, it is impossible to judge an entire area. It is essential to perform this locally to ensure the considered statistical description is (locally) homogeneous. The influence of noise is significant and contaminating very fast at small scales. In retrospect, this also demonstrates that the original column density map is very clean because if it were noisy we would not see the signal as it is. Otherwise, the WST and RWST signal would be swamped.

Acknowledgements. It has been a difficult time, I would like to thank my supervisor, Dr. Francois LEVRIER for his invaluable feedback and advice, as well as his time spent during consultations with me throughout my project.

References

[1] Allys et al., A&A **629**, A115 (2019).
[2] Bedionita et al., Sensors **19**, 1790 (2019.).
[3] Bron et al., A&A **610**, A12 (2018).
[4] Bruna, J. & Mallat, IEEE transactions on pattern analysis and machine intelligence **35**, 8 (2013).
[5] Cohen et al., Wavelets and multiscale signal processing (Springer) (1995).
[6] Draine, Physics of the Interstellar and Intergalactic Medium (Princeton University Press) (2011).
[7] Gratier et al., A&A **599**, A100 (2017).
[8] Lombardi et al., A&A **566**, A45 (2014).
[9] Pety et al., A&A **605**, A100 (2017).
[10] Sifre et al., IEEE Conference on Computer Vision and Pattern Recognition (CVPR), 1233-1240 (2013).
[11] Goodman et al., Astrophys. J **692**, 91-103 (2009).
[12] https://www.wikiwand.com/en/Orion_Molecular_Cloud_Complex

Appendix A Morlet wavelets

The Morlet wavelet is a product of a complex exponential multiplied by a Gaussian window with width

σ. In one-dimension, the Morlet wavelets are defined by:

$$\psi(x) = \alpha(e^{ix} - \beta)\ e^{-x^2/(2\sigma^2)} \tag{12}$$

where α and $\beta = exp(-\sigma^2/2)$ are normalized factors. The wavelets are constructed by dilation from an initial wavelet in 1D:

$$\psi_j(x) = 2^{-2j}\psi(2^{-j}x) \tag{13}$$

Assuming β may be neglect ($\sigma > 1$), the Fourier transform of the wavelet ψ_j is centered on the wavenumber 2^{-j} and a bandwith proportional to $(2^j\sigma)^{-1}$ [1]. In two dimensions, the wavelets are built by rotation and dilation [1]:

$$\psi(\mathbf{x}) = \alpha(e^{i\mathbf{n}\cdot\mathbf{x}} - \beta)\cdot e^{-|\mathbf{x}|^2/(2\sigma^2)}, \tag{14}$$

where $\mathbf{n}$ is a normalized vector giving the oscillation direction of the mother wavelet in (x, y) plane. The center and width of the Fourier transform of such a wavelet are determined by rotations and scaling [1].

Appendix B The energy of the field $I(\mathbf{x})$

The WST provides a formula to estimate the field energy [4]:

$$\|I\|^2 = S_0^2 + \sum_{j_1,\theta_1} S_1^2(j_1,\theta 1) + \sum_{j_1,\theta_1,j_2,\theta_2} S_2^2(j_1,\theta_1,j_2,\theta_2) + \epsilon, \tag{15}$$

where

$$\|I\|^2 = \frac{1}{\mu_0^2}\int |I(\mathbf{x})|^2 d^2x. \tag{16}$$

The term ϵ represents the energy in the layers $m \geqslant 3$ containing less than 1% of the total energy [4]. The set of values j_i and θ_i shows that wavelets cover the whole spectrum of the field. The conservation of energy is written at the level of the power spectrum of the field at the oriented scale (j_1, θ_1) [1]:

$$\|I * \psi_{j_1,\theta_1}\|^2 = S_1^2(j_1,\theta_1) + \sum_{j_2,\theta_2} S_2^2(j_1,\theta 1, j_2,\theta_2) + \epsilon', \tag{17}$$

where $\|I * \psi_{j_1,\theta_1}\|^2$ is defined similarly to $\|I\|^2$. The term ϵ' also encodes the energy contained in the $m \geqslant 3$ layers that have been shown to be negligible for stationary processes [4].

Appendix C Additional sets of results

We give in this appendix additional sets of RWST coefficients for the layer m = 1 and m = 2. The Fig.8 and 9 show the terms of the RWST coefficients of layer m = 1 and m = 2 for five subsets in the absence of noise. The plot of the $\widehat{S}_1^{iso}$, $\widehat{S}_1^{aniso}$, $\theta^{ref,1}$ terms of the RWST coefficients for m = 1 and the $\widehat{S}_2^{iso,1}$, $\widehat{S}_2^{iso,2}$, $\widehat{S}_2^{aniso,1}$, $\widehat{S}_2^{aniso,2}$, $\theta^{ref,2}$ terms of the RWST coefficients for m = 2 are given in Fig.10 and Fig.11 when adding noise with SNR = 10, 1, 0.1 and 0.001. These figures Fig.12 and Fig.13 recast the $m = 1$ RWST coefficients in order to show how they change with carying SNR. Similar plots are presented in Figs.14 to Fig.17 for the $m = 2$ RWST coefficients.

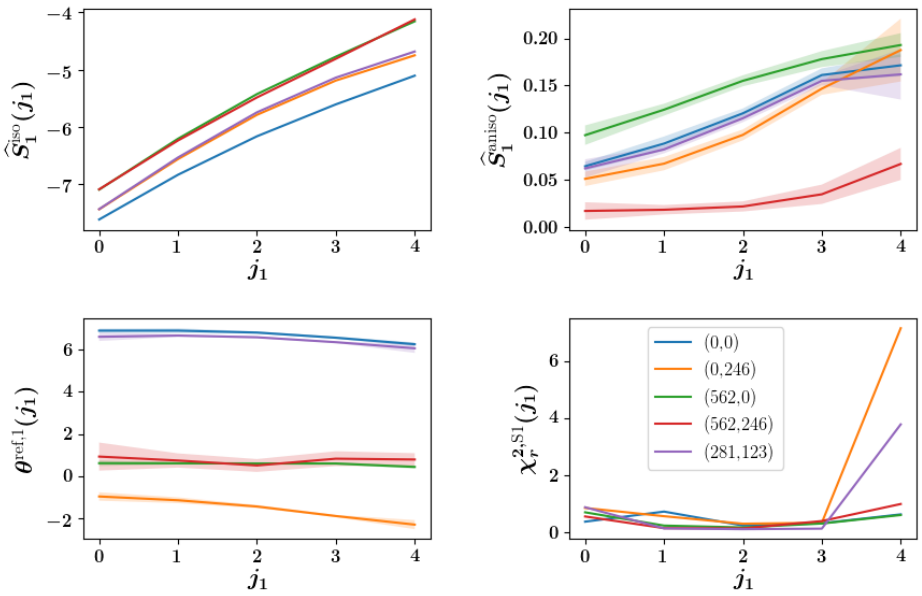

Fig. 8. The $\widehat{S}_1^{iso}$, $\widehat{S}_1^{aniso}$, and associated $\theta^{ref,1}$ terms of the RWST coefficients for five subsets in the absence of noise.

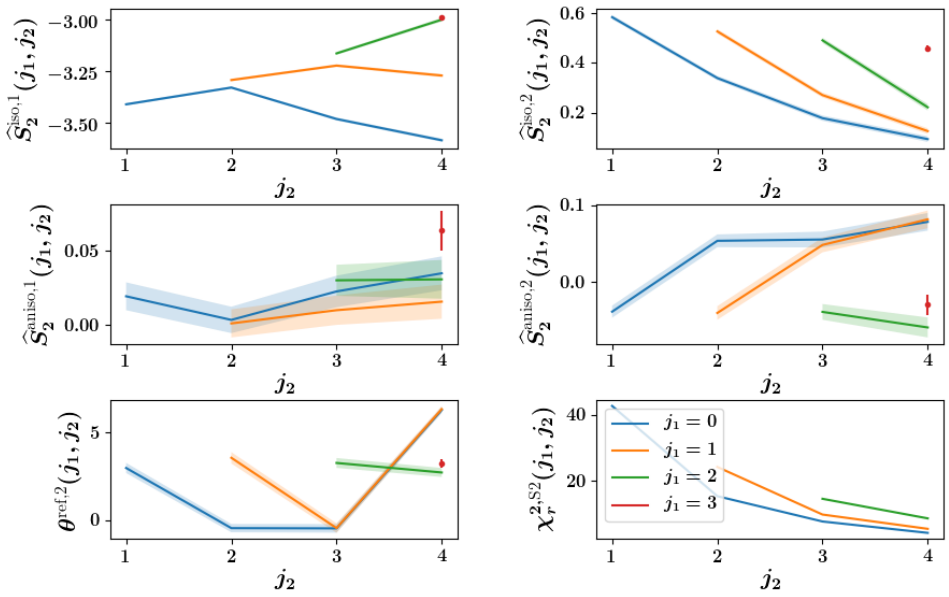

Fig. 9. The $\widehat{S}_2^{iso,1}$, $\widehat{S}_2^{iso,2}$, $\widehat{S}_2^{aniso,1}$, $\widehat{S}_2^{aniso,2}$, and associated $\theta^{ref,2}$ terms of the RWST coefficients for five subsets in the absence of noise.

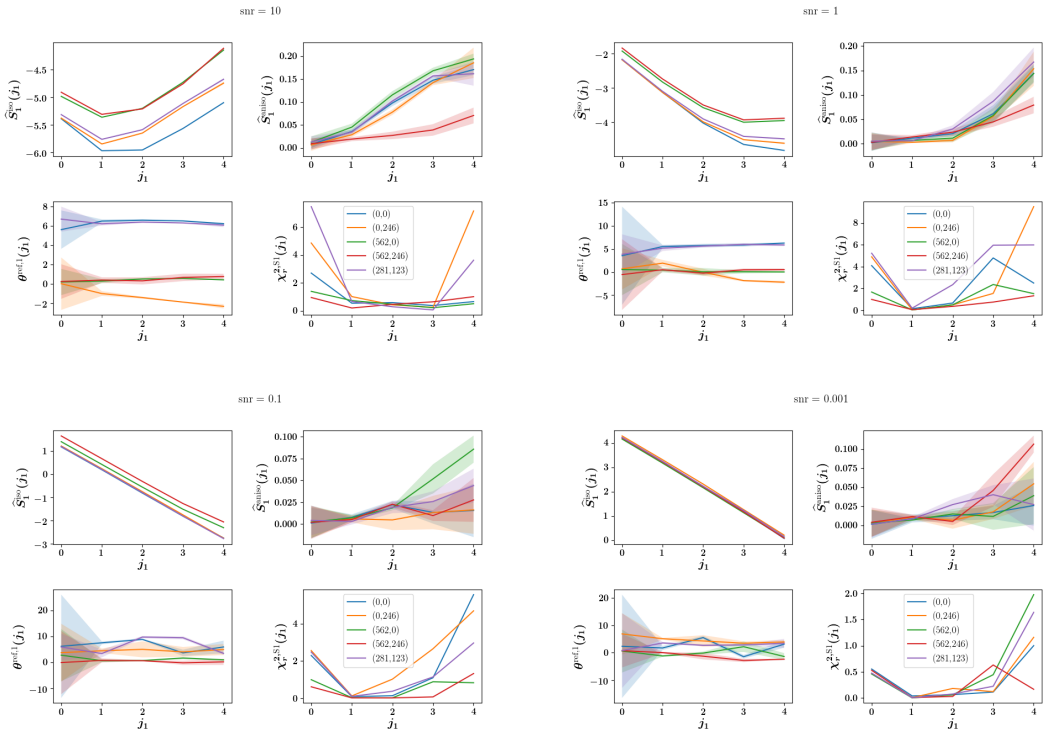

Fig. 10. Plots of $\widehat{S}_1^{iso}$, $\widehat{S}_1^{aniso}$, and associated $\theta^{ref,1}$ terms of the RWST coefficients in the presence of noise with SNR = 10, 1, 0.1, 0.001.

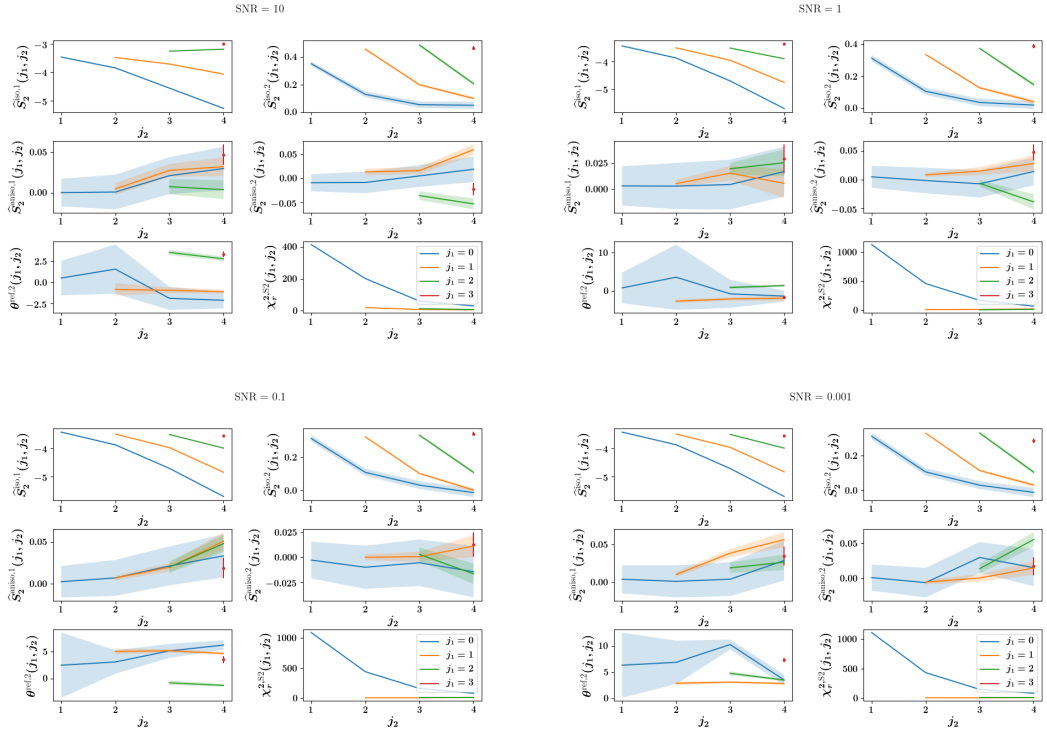

Fig. 11. Plots of $\widehat{S}_2^{iso,1}$, $\widehat{S}_2^{iso,2}$, $\widehat{S}_2^{aniso,1}$, $\widehat{S}_2^{aniso,2}$, and associated $\theta^{ref,2}$ terms of the RWST coefficients m = 2 in the case of presence with SNR = 10, 1, 0.1, 0.001.

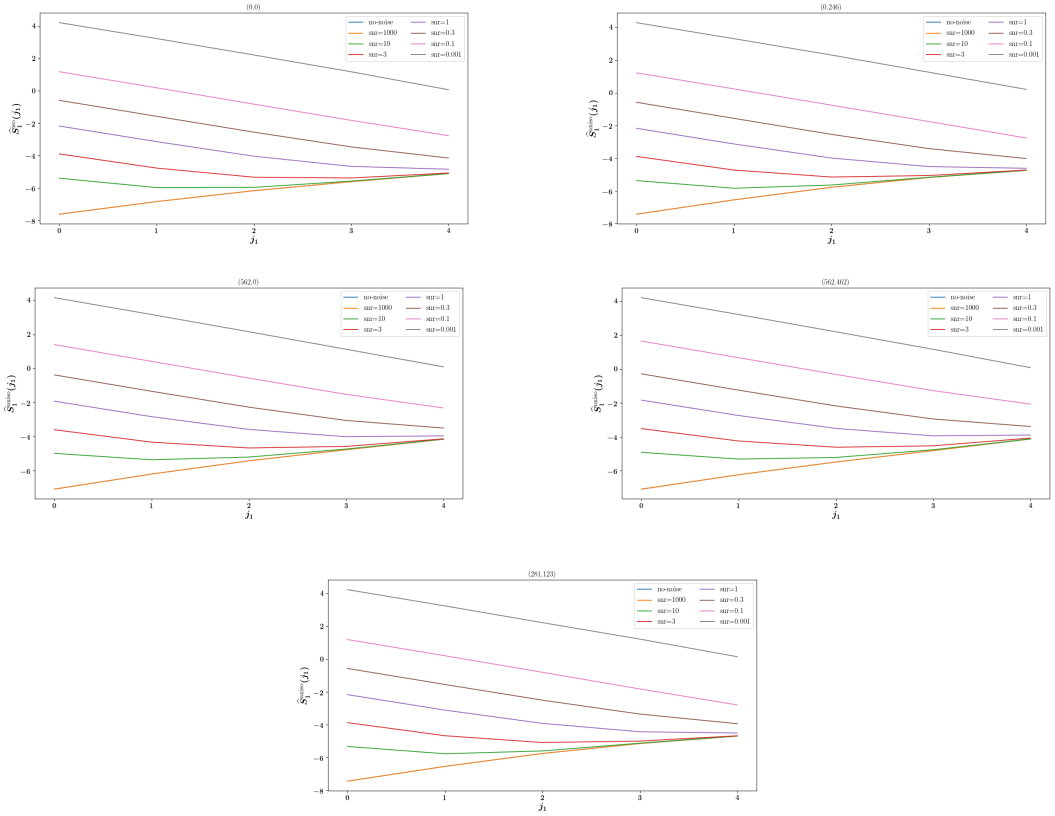

Fig. 12. Plots of $\widehat{S}_1^{iso}$ terms of the RWST coefficients for various values of the SNR. The shape of curves are the same for the five subsets.

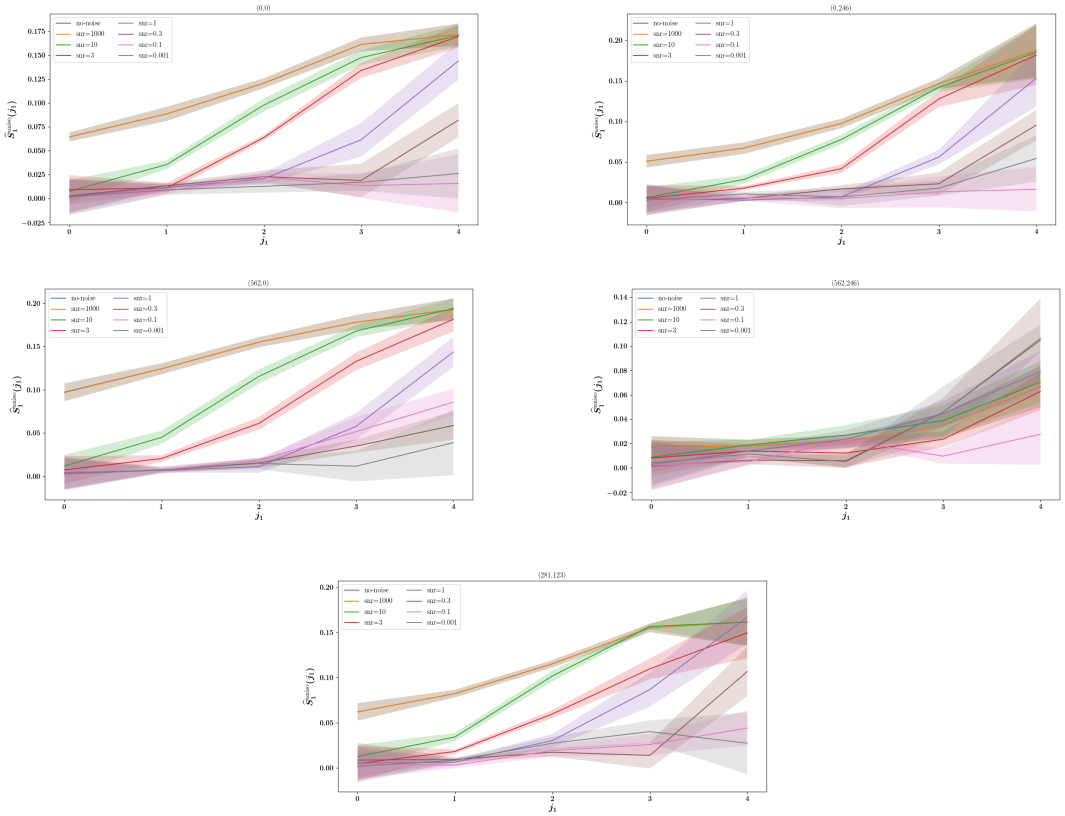

Fig. 13. Plots of $\widehat{S}_1^{aniso}$ terms of the RWST coefficients for various values of the SNR.

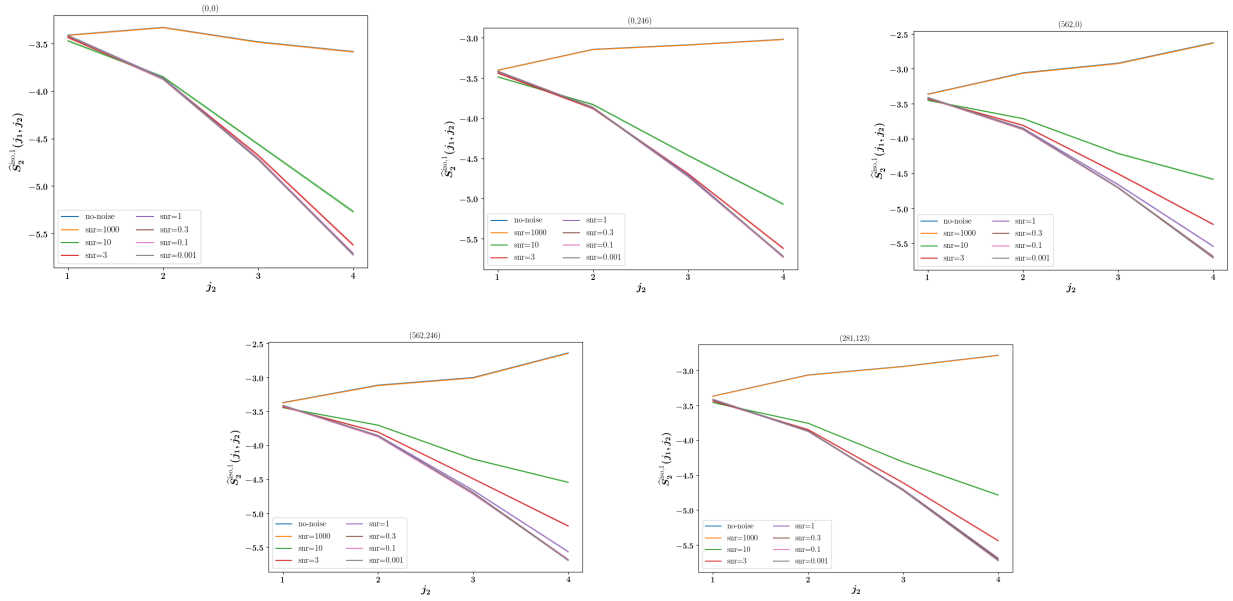

Fig. 14. Plots of $\widehat{S}_2^{iso,1}$ terms of the RWST coefficients for various values of the SNR. The shape of curves are vary similar for the five subsets.

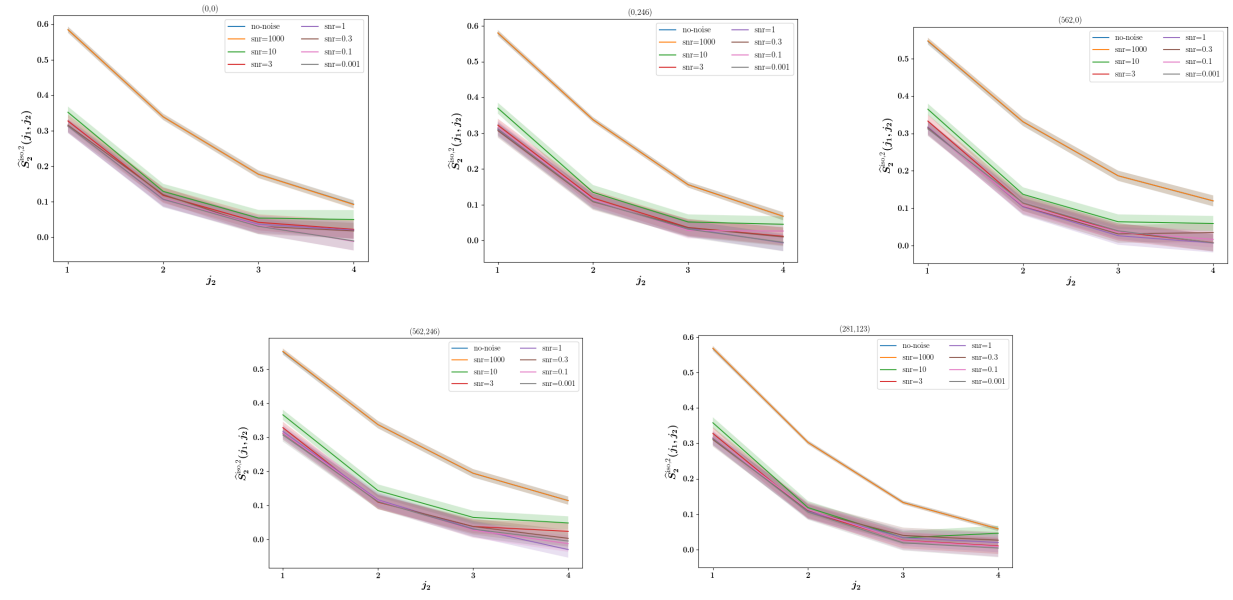

Fig. 15. Plots of $\widehat{S}_2^{iso,2}$ terms of the RWST coefficients following the values of SNR. The shape of curves do not change in the five subsets.

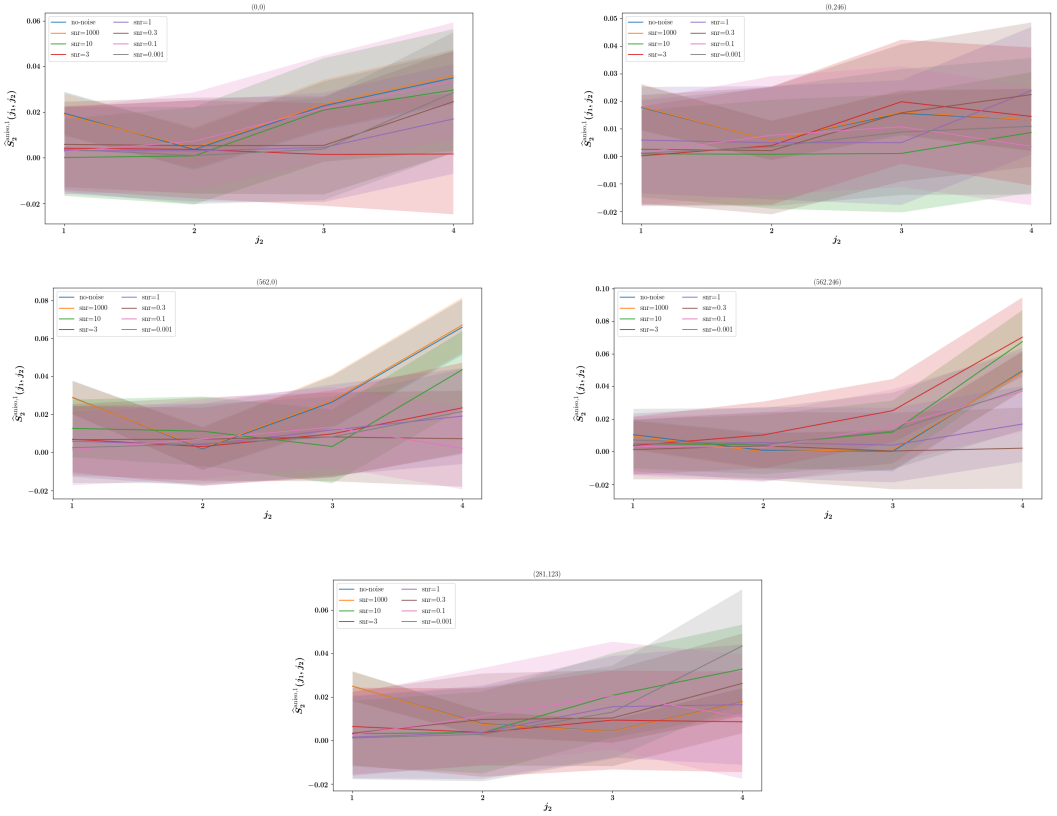

Fig. 16. Plots of $\widehat{S}_2^{aniso,1}$ terms of the RWST coefficients for various values of the SNR.

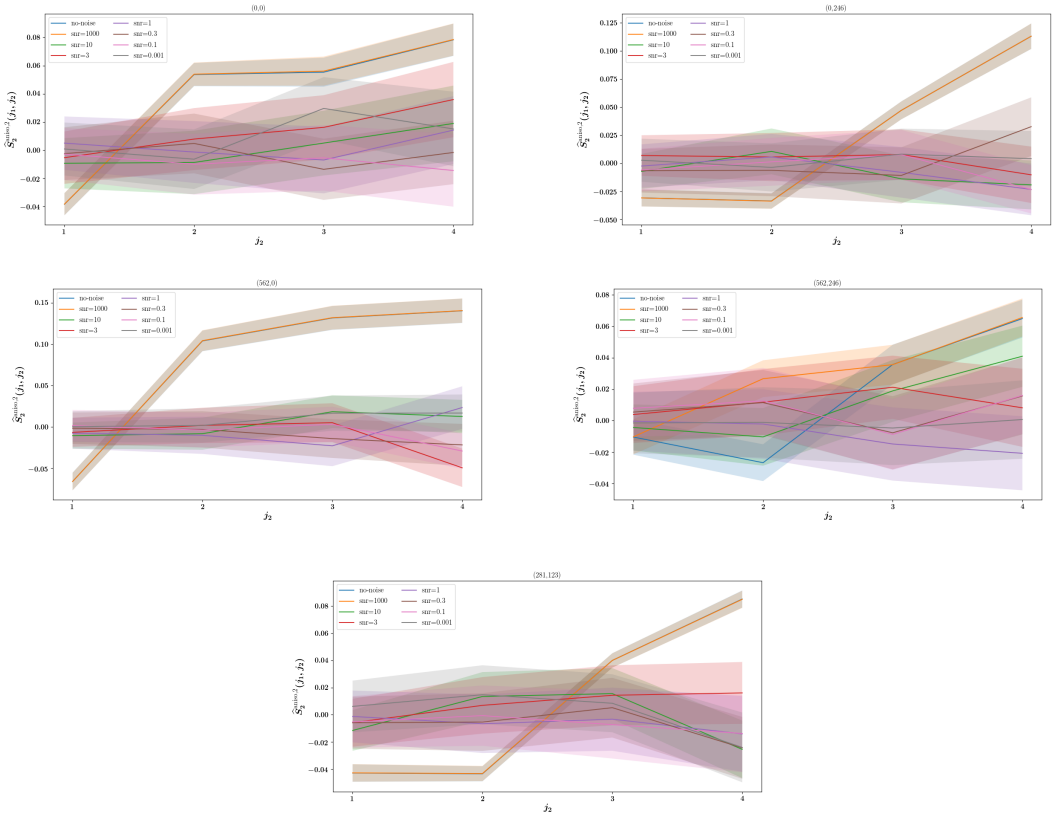

Fig. 17. Plots of $\widehat{S}_2^{aniso,2}$ terms of the RWST coefficients for various values of the SNR.